PLOS ONE

RESEARCH ARTICLE

A fluidics-based impact sensor

Daigo Takahashi, Keisuke Hara, Taiji Okano, Hiroaki Suzuki*

Faculty of Science and Engineering, Chuo University, Tokyo, Japan

* suzuki@mech.chuo-u.ac.jp

Abstract

Microelectromechanical systems (MEMS)-based high-performance accelerometers are ubiquitously used in various electronic devices. However, there is an existing need to detect physical impacts using low-cost devices with no electronic circuits or a battery. We designed and fabricated an impact sensor prototype using a commercial stereolithography apparatus that only consists of a plastic housing and working fluids. The sensor device responds to the instantaneous acceleration (impact) by deformation and pinch off of a water droplet that is suspended in oil in a sensor cavity. We tested the various geometrical and physical parameters of the impact sensor to identify their relations to threshold acceleration values. We show that the state diagram that is plotted against the dimensionless Archimedes and Bond numbers adequately describes the response of the proposed sensor.

Citation: Takahashi D, Hara K, Okano T, Suzuki H (2018) A fluidics-based impact sensor. PLoS ONE 13(4): e0195741. https://doi.org/10.1371/journal.pone.0195741

Editor: Yogendra Kumar Mishra, Institute of Materials Science, GERMANY

Received: December 28, 2017

Accepted: March 28, 2018

Published: April 10, 2018

Data Availability Statement: All relevant data are within the paper and its Supporting Information files.

Funding: This research was supported by JKA and its promotion funds from KEIRIN RACE (27–120). The funders had no role in study design, data collection and analysis, decision to publish, or preparation of the manuscript.

Competing interests: This research was supported by JKA and its promotion funds from KEIRIN RACE (27–120). The funders had no role in study design, data collection and analysis, decision to publish, or preparation of the manuscript. This does not alter

Introduction

Silicon-based solid-state accelerometers are ubiquitously used nowadays in various consumer electronic devices such as automobiles, smartphones, video games, and wearable equipment [1–5]. Because MEMS devices are well suited for integration in electronic circuits, physical acceleration data converted to electronic signals are often processed by the computer, stored in memory, and transmitted to other devices, depending on the applications [6–8].

However, there is a need for a device to detect acceleration in an easier manner and at a lower cost without the use of electronics or a battery. For instance, in logistics, customers want to know whether their packages have been delivered safely and that they have not been dropped or crushed. Modern MEMS accelerometers are equipped with a data logger and memory, but they are still costly, and they have been only used for the delivery of special items. Another need for an accelerometer is in sports. In many contact sports, injuries (e.g., head injuries, concussions) often arise from physical contacts, such as in American football [9], rugby [10, 11], ice hockey [12, 13], basketball, soccer [14, 15], judo [16], and many others. Today, MEMS-based sensors have been developed specifically for these sports [17], and are sold in the market [11, 18, 19]. These are used to monitor impacts mostly in well-funded professional and top-level college sports [12, 13, 20, 21]. When a severe impact occurs on an athlete's head, the player is withdrawn from the game or practice, and is advised to undergo a medical check. Correspondingly, these sensors can be also utilized for gathering statistical data for impacts during sports, which are then analyzed to allow enforcement of appropriate safety measures [22–25]. Considering that in many sports the practice and game plans are decided

our adherence to PLOS ONE policies on sharing data and materials.

based on experimental grounds, statistical data should be gathered and used even in recreational, amateur, high-school, youth, and children's sports [15, 19, 26–30]. MEMS wearable devices specialized for sports are still too expensive to be used by the majority of players, or in every sports scene [17, 18, 20, 31].

For these destined applications, precision in the recorded acceleration values, or the data time resolution, need not be very high. It is often sufficient to know whether or not a recorded acceleration surpasses a certain threshold value. In transportations, use of such a simple and low-cost device ensures the safety of the package throughout its logistical processing. In sports, it becomes possible to comprehend the statistics of dangers associated with daily practices and games and to encourage a player who has experienced jolts to seek medical care.

In this work, we propose a simple binary sensor that only consists of a plastic housing and working fluids to detect instantaneous acceleration (impact). In this sensor, a water droplet serves as the inertial proof mass. The droplet is suspended in oil and is deformed by acceleration, thereby allowing it to be eventually pinched off. Several research studies have been conducted to develop fluidics-based inertial sensors, but they still use complicated structures and electronic readouts [32–35]. Herein, we fabricated an extremely simple impact sensor in which the readout is based on the visual judgment, using a commercial stereolithography apparatus. No electronic circuit or battery is necessary so that it can be cost-effective and process-effective in mass production, leading to its widespread use in various applications. We show that our prototype sensor was able to detect the g values ranging from 30 to 150 g with a duration of ~10 ms. By changing the physical parameters of its design and working fluids, we investigated the physical principles underlying the function of the fluidics-based sensing device.

Sensing principle

We fabricated the rectangular housing with a hollow cylindrical cavity with a narrow neck (constriction) in the middle, as seen in Fig 1(A). This cavity is filled with oil, and a water droplet immersed in it serves as a proof mass. The droplet is carefully placed on one side of the neck. Owing to the interfacial tension, the water droplet does not readily move across the neck when the device is at rest. When an acceleration or an impact is exerted on the device parallel to the axis of the cylindrical cavity, an inertial force is exerted on the water droplet relative to the surrounding oil as there is a density difference between oil and water. As a result, part of the water droplet deforms and enters into the constriction. When the acceleration is large enough, the water droplet is elongated and is pinched off. Herein, the direction of the droplet movement depends on the density difference. When a hydrocarbon-based oil is used (relative density ρ_{medium} = 0.6–0.8 g/L), the droplet moves toward the direction of the impact (Fig 1B). However, when fluorocarbon-based oil (ρ_{medium}~1.8 g/L) is used, the droplet moves in a direction opposite to the acceleration (Fig 1C). The separated small droplet moves to the other side of the constriction and is readily detected by human eyes. The threshold for the movement of the droplet depends on various physical parameters, such as the diameter of the constriction, density difference, interfacial tension between fluids, and viscosity of fluids.

Materials and methods

Fabrication process

We fabricated the housing of the prototype device using a commercial stereolithography apparatus (Form2, Formlabs) equipped with a 405-nm violet laser (φ = 140 μm laser spot) and a layering thickness of 50 μm, according to the manufacturer's protocol. The process flow is depicted in Fig 2(A). In short, we designed the device with a 3D CAD software (Rhinoceros 5.0). The design was saved in a file which was converted in the .stl format for processing by the

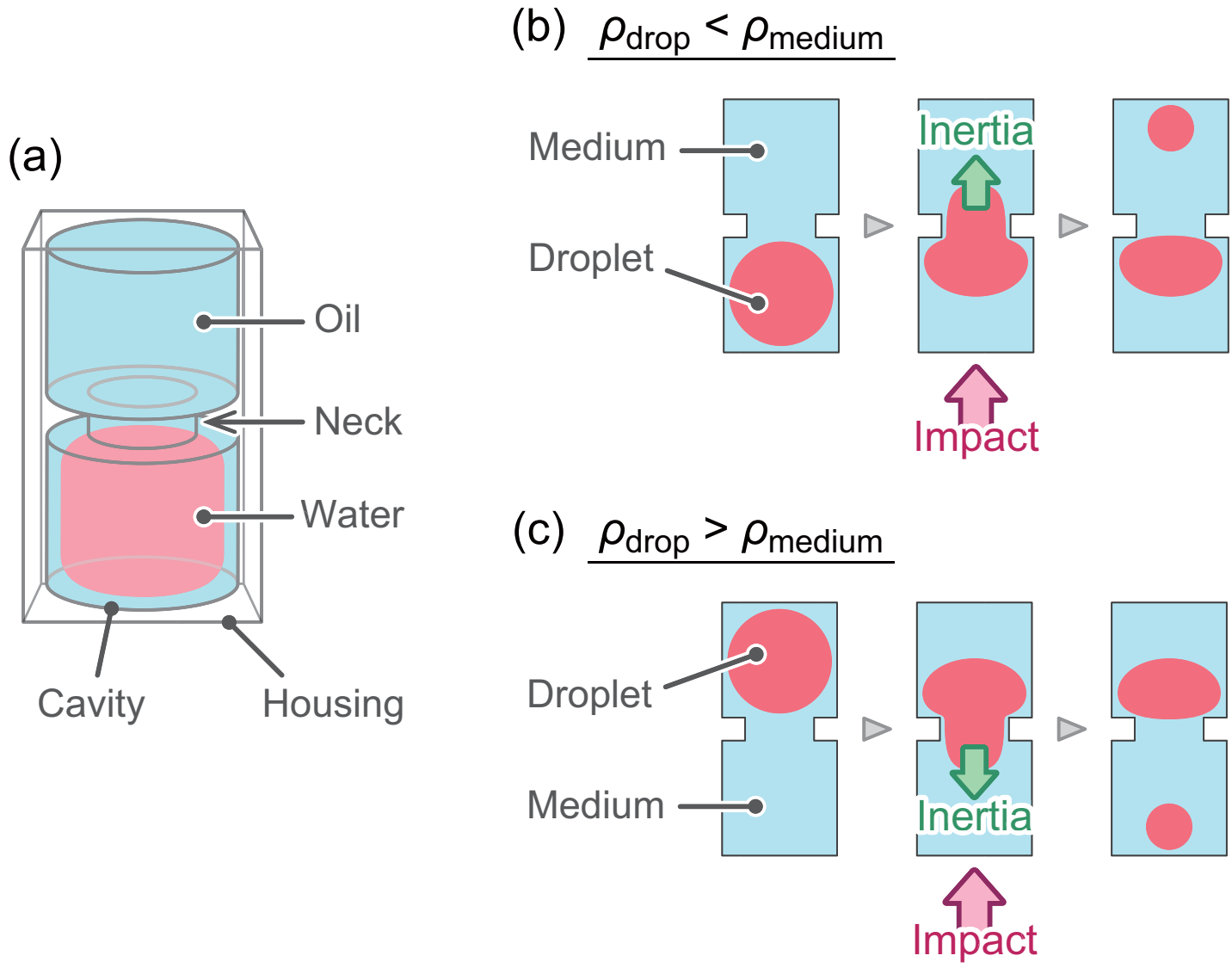

Fig 1. Schematics of the fluidic based impact sensor. (a) Schematic overview of the basic structure of the sensor. (b, c) Working principle of the sensor based on which impacts are detected depending on different combinations of immiscible working fluids.

https://doi.org/10.1371/journal.pone.0195741.g001

apparatus. The device consisted of a main housing with a hollow cylindrical cavity and two lids. After the lithography process, the device was removed from the stage and uncured resin was washed with isopropanol. After drying, supporting pillars were removed manually using nippers. After closing one side of the cavity using one of the lids, we applied the amorphous fluorinated polymer CYTOP in the internal wall of the cavity to make it highly hydrophobic. It was completely dried by baking at a temperature of 160˚ for 1 h in the furnace. We confirmed that the contact angle (CA) of the native resin in air increased from 71˚ to 96˚ after the CYTOP treatment.

We then injected the fluorocarbon oil and 65 μl of colored water using a pipette. We then sealed another side of the cylinder using another lid carefully so that the air bubble was not trapped in the cavity. In the initial stage of the development, we also tested the hydrocarbon oil (such as mineral oil and liquid paraffin), but found that the fluorocarbon was more suitable

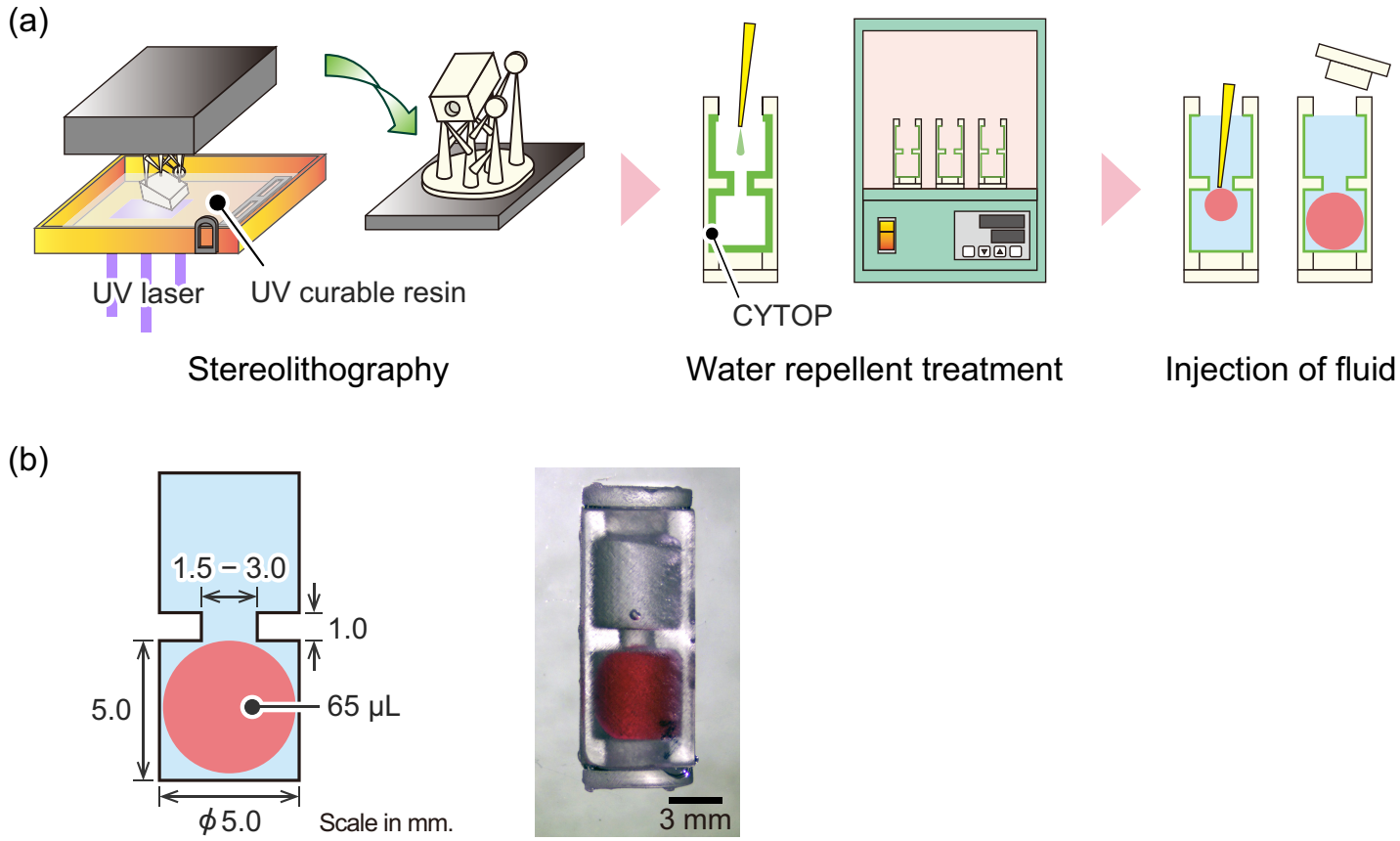

Fig 2. Fabrication and design of the impact sensor. (a) Fabrication process flow. (b) Actual design in cross section, and an image rendition of the complete sensor.

https://doi.org/10.1371/journal.pone.0195741.g002

because it had a large density difference from water. Thus, we employed commercial fluorocarbon oil (FC-40 and FC-770, 3M) as the basic surrounding medium.

The outer dimensions of the device are $6 \times 6 \times 16$ mm^3 and have two hollow cylindrical cavities with a 5-mm inner diameter and a 5-mm height on both sides (Fig 2B). These large cavities are connected by a narrow channel (neck or constriction) with an inner diameter of 1.5 –3.0 mm and a length of 1 mm. A photograph of the completed device is shown in Fig 2(B).

Falling test apparatus

We tested the response of our fluid-based impact sensor in accordance to the falling test using the custom-made setup shown in Fig 3(A). We fixed our sensors together with the commercially available three-axis MEMS accelerometer—equipped with Wi-Fi data transmission (MA3, Microstone, Japan)—to the metal case that consisted of two pieces of channel-type aluminum bars connected by a hinge. This object (dimensions: $50 \times 50 \times 370$ mm, total mass: 600 g) was subjected to a free fall through a 75-mm inner diameter PVC pipe (guide pipe). Because the diagonal size of the housing was 70.7 mm, the housing fell vertically. The object fell from various heights onto a 20-mm thick polyethylene sheet.

MEMS accelerometers that are designed for contact sports that are available in the market are designed to detect accelerations above 50 g, and most of the published research papers on this topic indicate that accelerations higher than approximately 100 g can possibly cause traumatic head injuries or concussion [20, 21, 36, 37]. Thus, we decided to set the detection range of our sensor to 30–150 g.

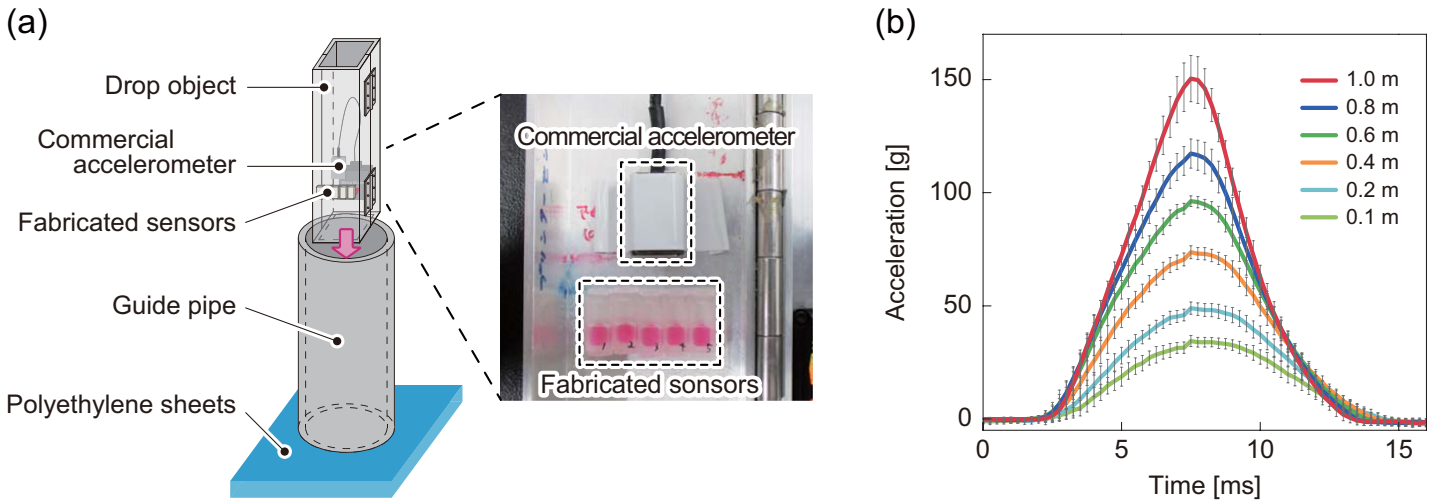

Fig 3. Falling test apparatus. (a) Custom-made apparatus consisting of drop object, guide pipe, and polyethylene sheet. (b) Temporal acceleration profiles of the object dropped from different heights (0.1–1.0 m) measured by the commercial accelerometer.

https://doi.org/10.1371/journal.pone.0195741.g003

Prior to the experiment, we evaluated our handmade apparatus. The raw signal generated from the commercial accelerometer, averaged over five independent falling experiments at each height, is shown in Fig 3(B). This result shows that our falling test apparatus is able to generate reproducible acceleration profiles in the acceleration range of 30–150 g within a time period of ~10 ms. This period is defined as the time difference between the rising and falling signal edges at 0 g (the peak acceleration value and the duration of each falling height are shown in S1 Fig). This duration is also a typical value reported in contact sports, such as in American football hits [20, 30, 38], soccer head contacts [39], and judo waza [16] in accordance to the literature.

Results and discussion

There are several parameters that determine the threshold of impact detection. As wider the diameter of the neck and the strength of the interfacial tension of immiscible fluids decrease, the deformation of the water droplet also increases. As the density difference between immiscible fluids increases, the relative inertia force increases. Additionally, as the viscosity values of the fluids are increased, the deformation of the water droplet occurs within a shorter time period. We carefully studied the influence of each of these parameters, as outlined below.

Effect of neck diameter

We tested the inner diameters of the neck d_{neck} to be 1.5, 2.0, 2.5, and 3.0 mm. When the droplet remained unchanged after a fall, we considered that the sensor did not respond. When at least one part of the droplet separated from the "mother droplet" and moved to the other side of the neck, we considered that the sensor responded. Fig 4(A) shows the fraction of the sensors that responded when tested at various falling heights. That is, when at least one part of the water droplet moved to the other side in three of the five tested sensors, the success fraction was 60%. We repeated the falling tests at various heights, and plotted the fraction versus peak acceleration value (g_{peak}) obtained from the MEMS accelerometer profile. The result was fitted

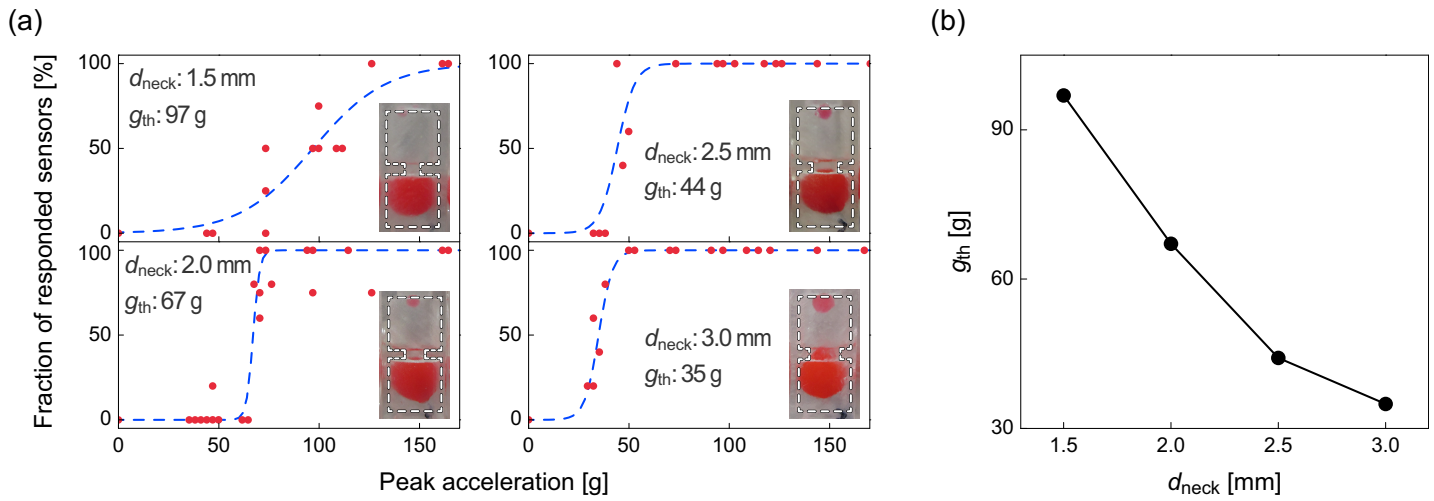

Fig 4. Result of the impact sensors with different neck diameter d_{neck}. (a) Fraction of responded sensors versus peak acceleration values with d_{neck} = 1.5–3.0 mm. Insets show typical images of responded states after droplet falls. Blue dashed lines represent the fitted curves based on the use of the sigmoidal function. (b) Plot showing the dependence of g_{th} on d_{neck}.

https://doi.org/10.1371/journal.pone.0195741.g004

with the sigmoidal function, which is often used for modeling the stepwise behavior; i.e.,

$$f(g_{peak}) = \frac{1}{1 + \exp\{-k(g_{peak} - g_{th})\}}, \quad (1)$$

where k and g_{th} are fitting parameters. The threshold g_{peak} value of the sensor was determined as the inflection point g_{th} of the curve. This nonlinear fitting was performed based on the least-squares-method using the solver in Microsoft Excel (see S1 Table for all parameter-fitting results). As seen in Fig 4(A), the neck diameter had a significant effect on the g_{th} values. The variable g_{th} is plotted as a function of d_{neck} in Fig 4(B). As the inner diameter increases, the threshold decreases. At the smallest neck diameter (d_{neck} = 1.5 mm) the slope of the fitting function is small, while a steep change is elicited with $d_{neck} \geq 2.0$ mm. This result indicates that the detection becomes sensitive to small variations, and stochastic at small values of d_{neck}. Moreover, as observed in the typical images in the insets, at d_{neck} = 1.5 mm, the detached droplet that moved to the other side was too small to be recognized with naked eyes. The diameter of the separated droplet was mainly depended on d_{neck} (S2 Fig).

The present result indicates that g_{th} can be easily adjusted by the neck diameter d_{neck}, but reproducibility and visual recognition can be compromised in high impact detections at small d_{neck} values. Thus, we decided to employ the device using d_{neck} = 2.0 or 3.0 mm in the conducted experiments, as described next.

Effect of viscosities of working fluids

When the impact was applied to the water droplet, it deformed and penetrated the neck region. The viscosities of both fluids (water and oil) are expected to affect g_{th} because increased viscosity restricts the deformation within a given time. The physical constants of the working fluid tested in this work are listed in Table 1.

First, we tested different fluorocarbon oils using pure water. FC-40 and FC-770 have similar densities but different viscosities (4.1 and 1.4 mPa·s, respectively). The result tested with the device with d_{neck} = 2.0 mm is shown in Fig 5. As expected, we obtained smaller g_{th} values with

Table 1. Density, dynamic viscosity, and kinematic viscosity, of working fluids [40].

	Type of fluid	Density $\times 10^3$ kg/m^3	Dynamic viscosity $\times 10^{-3}$ Pa·s	Kinematic viscosity $\times 10^{-6}$ m^2/s
Oil phase	FC-770	1.85	1.40	0.76
	FC-40	1.78	4.10	2.30
Aqueous phase (droplet)	Water	1.00	1.00	1.00
	45% sucrose	1.19	9.40	7.89
	65% sucrose	1.30	147	113
	70% sucrose	1.33	482	362
	60% glycerol	1.14	11.0	9.64
	90% glycerol	1.22	220	180
	100% glycerol	1.25	1410	1130

https://doi.org/10.1371/journal.pone.0195741.t001

less viscous oils. The threefold difference of the oil viscosity yielded an approximate twofold difference in g_{th}.

We subsequently tested the increased viscosity of the water droplets by adding either sugar (sucrose) or glycerol. The density and viscosity of these mixtures was obtained from the handbook, as described in Table 1. The elicited responses at d_{neck} = 2.0 or 3.0 mm with FC-40 as the oil phase are shown in Fig 6.

Both 45 wt% sucrose and 60 wt% glycerol aqueous solutions had viscosities that were approximately 10 times higher than pure water. Based on these tests, we obtained similar responses: g_{th} = 30–50 g for d_{neck} = 3.0 mm, and g_{th} = 70–90 g with d_{neck} = 2.0 mm (Fig 6(A) and 6(B), top). Because the g_{th} values of pure water are 67 g and 35 g, respectively, for 2.0 and 3.0 mm neck diameters, the effect of the water phase viscosity was not as significant as the oil viscosity. Subsequently, 65 wt% sucrose and 90 wt% glycerol solutions are more viscous than water by approximately 100 times. In these cases, the value of g_{th} for a device with d_{neck} = 3.0

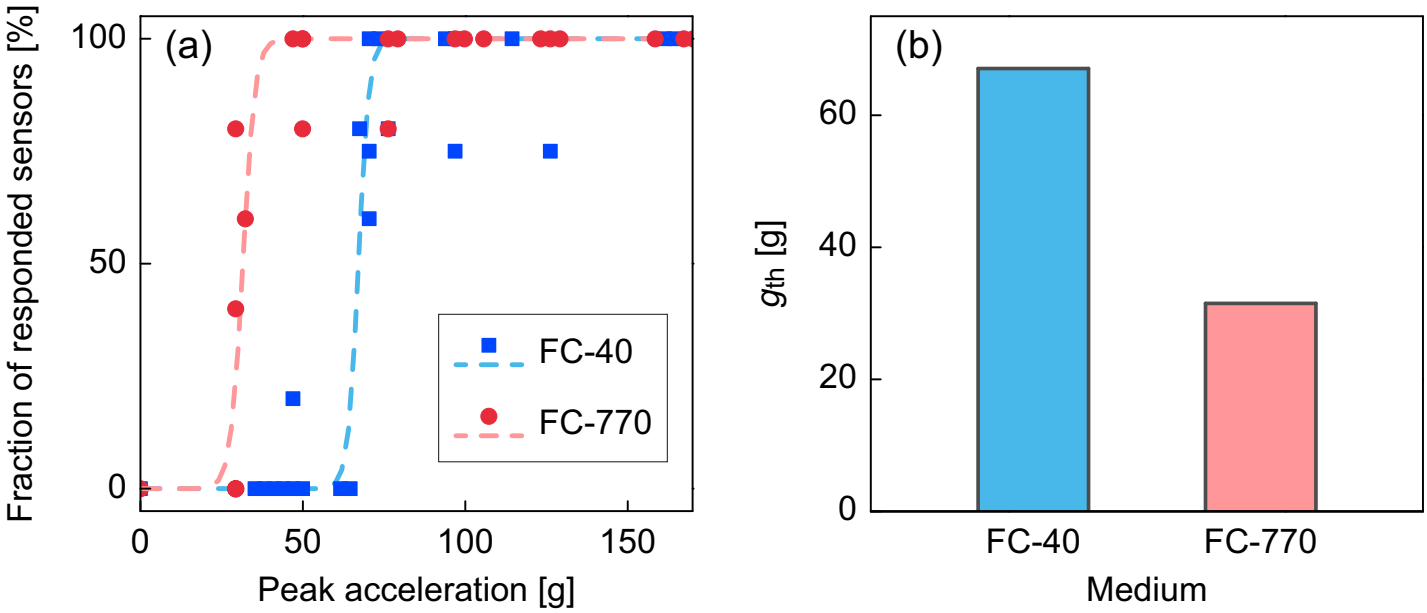

Fig 5. Result of the impact sensor with different oil phase. (a) Fraction of responded sensors versus peak acceleration tested using different oil viscosities. (b) Comparison of g_{th} for fluorocarbon oils with different viscosities.

https://doi.org/10.1371/journal.pone.0195741.g005

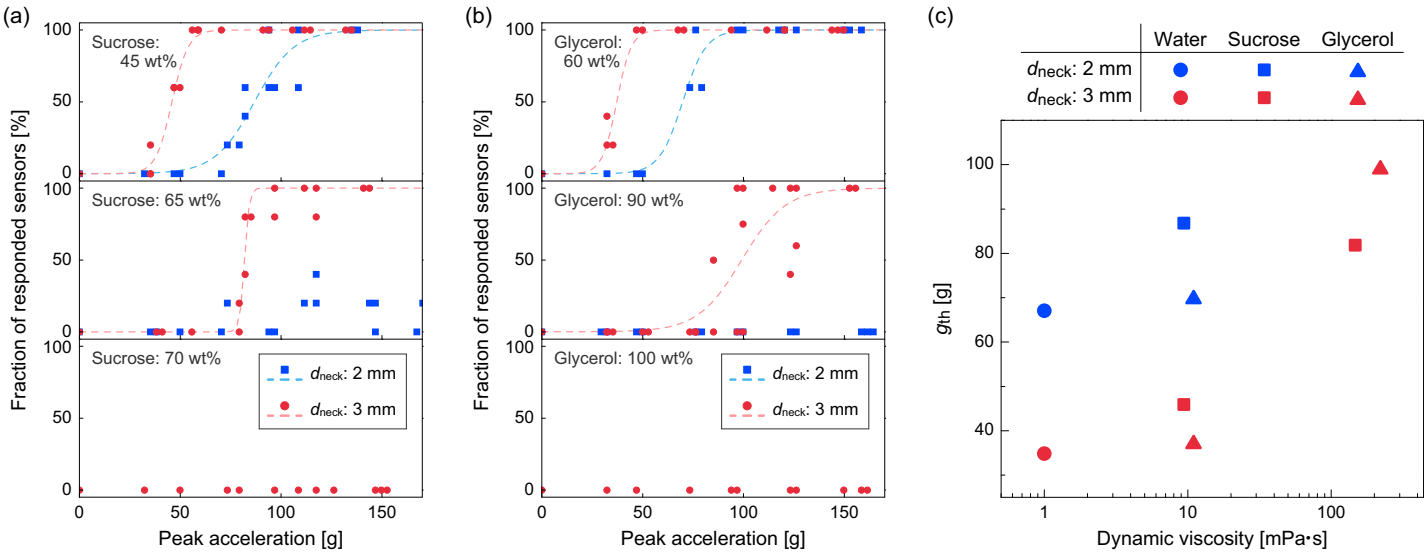

Fig 6. Results of the impact sensor with different aqueous solution (droplet). (a, b) Fraction of responded sensors versus peak acceleration tested at different water densities. (a) Sucrose solution (45–70 wt%), (b) glycerol solution (60–100%), and (c) dependence of g_{th} on water viscosity.

https://doi.org/10.1371/journal.pone.0195741.g006

mm was increased to 82 g and 99 g, respectively, whereas the fraction of the responded devices with d_{neck} = 2.0 mm was less than 40% when subjected to accelerations up to 150 g (Fig 6(A) and 6(B), middle). With 70 wt% sucrose solution and 100% glycerol solutions as the droplet, no sensor responded even with a d_{neck} value of 3.0 mm (Fig 6(A) and 6(B), bottom). These results indicate that the viscosity of the oil phase is more sensitive to the response of our sensor compared to that of the water phase. The dependencies of the g_{th} values on the viscosity of the water phase are summarized in Fig 6(C).

Effect of interfacial tension

The extent of the deformation of the water/oil interface in response to the inertial force should also depend on the interfacial tension $\gamma_{w/o}$. That is, larger $\gamma_{w/o}$ values tend to maintain the water droplet spherical, and smaller $\gamma_{w/o}$ values lead to a more elongated water droplet upon impact. We investigated this effect by varying $\gamma_{w/o}$ between FC-40 oil and water with the addition of alcohol. Mazutis and Griffiths [41] reported that addition of 10% and 40% ethanol to the water phase reduced the interfacial tension between the fluorocarbon oil and water (originally at 55.5 mN/m) to 35.3 and 16.1 mN/m, respectively. The experimental test was conducted with a device with d_{neck} = 2.0 mm, and is shown in Fig 7(A). The dependence of g_{th} on $\gamma_{w/o}$ (Fig 7B) shows that g_{th} is almost linearly dependent on $\gamma_{w/o}$ in the tested range.

Nondimensional analyses

Thus far, we have observed how the geometrical size of the neck and the material properties of working fluids alter the threshold acceleration value g_{th}. In fluid mechanics, dimensionless numbers describe the overall behavior of the system. For example, the microfluidic system in which water-in-oil droplets are formed by coaxial streams are characterized by the Weber number (*Wb*, ratio of hydrodynamic force to the surface tension force) and the capillary number (*Ca*, ratio of viscous force to the interfacial tension force). [42] The state diagram of flow modes that are plotted as a function of *Wb* and *Ca*, is shown to be separated into distinct regimes describing different flow modes (jetting and dripping).

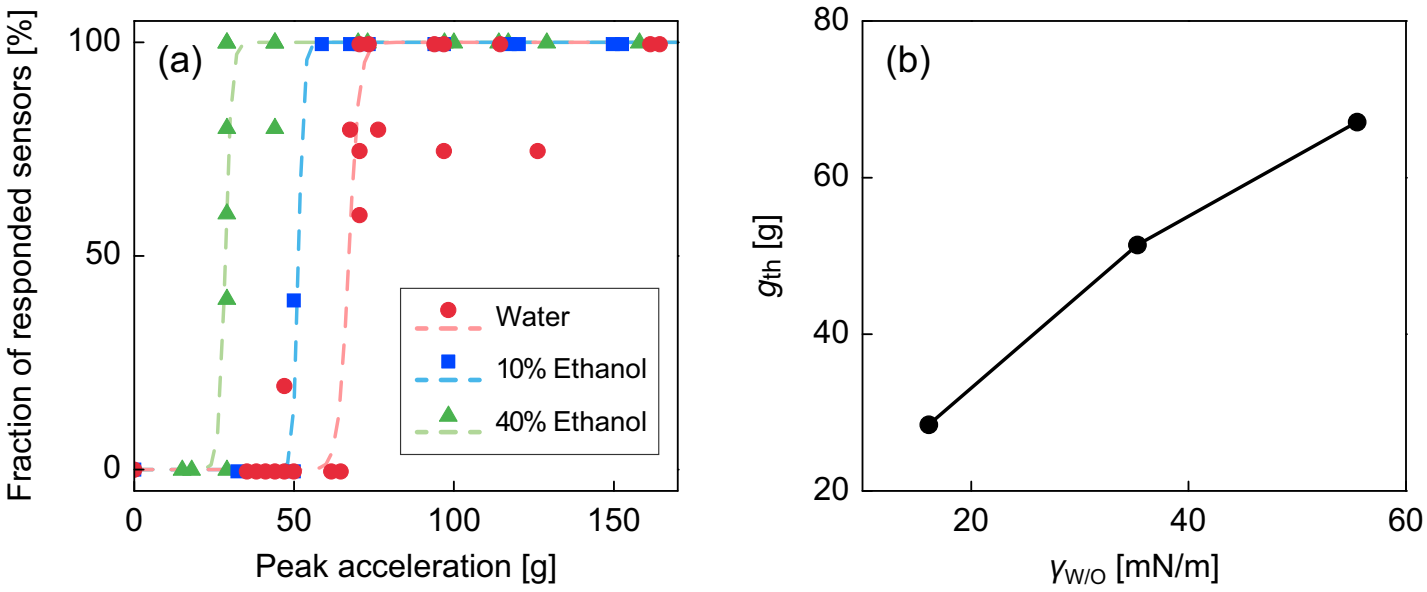

Fig 7. Results of the impact sensor with different interfacial tension. (a) Fraction of responded sensors versus peak acceleration tested at different interfacial tensions. (b) Dependence of g_{th} on $\gamma_{w/o}$.

https://doi.org/10.1371/journal.pone.0195741.g007

Although seemingly similar, we found that the use of *Ca* and *Wb* in the present system was inappropriate (S3 Fig). The hydrodynamic force in *Wb* and the viscous force in *Ca* are based on the premise that flow is in a steady state. However, in the present system, the dominant force that acts during the impact is the body force that is generated instantaneously as a result of the inertia. This consideration led to the use in these analyses of the Archimedes number *Ar*, the ratio of the external body force to the viscous force, and the Bond number *Bo*, the ratio of the external body force to the interfacial tension force. The definition and usage of these variables in our system are given by the following equations,

$$Ar = \frac{\rho_w \Delta\rho g_{\mathrm{peak}} d_{\mathrm{neck}}^3}{\mu_w^2} \tag{2}$$

and

$$Bo = \frac{\Delta\rho g_{\mathrm{peak}} d_{\mathrm{neck}}^2}{\gamma_{\mathrm{W/O}}} \tag{3}$$

where ρ and μ are the density and dynamic viscosity of the aqueous droplet, respectively, and $\Delta\rho$ is the density difference between water and oil. The state diagram is plotted in Fig 8, with open and filled symbols representing the conditions in which the sensors are classified as "did not respond" and "responded." Note that we employed the viscosity of the water droplet as the viscosity μ in *Ar*, because it can be readily tuned by adding sugar or glycerol. However, theoretically, it could be the viscosity of oil instead. The sets of symbols connected by solid or dashed lines belong to the same device and composition, but correspond to different g_{peak} values (fallen heights). It is obvious that at the high *Ar* regime ($10^4 < Ar < 10^7$), sensors responded when $Bo > 40$. This result means that when the body force owing to acceleration is high, the response of the fluid is determined by the constant value of the ratio of the body force and the interfacial tension. In the low *Ar* regime ($Ar < 10^2$) where the viscous drug is dominant, sensors ceased to

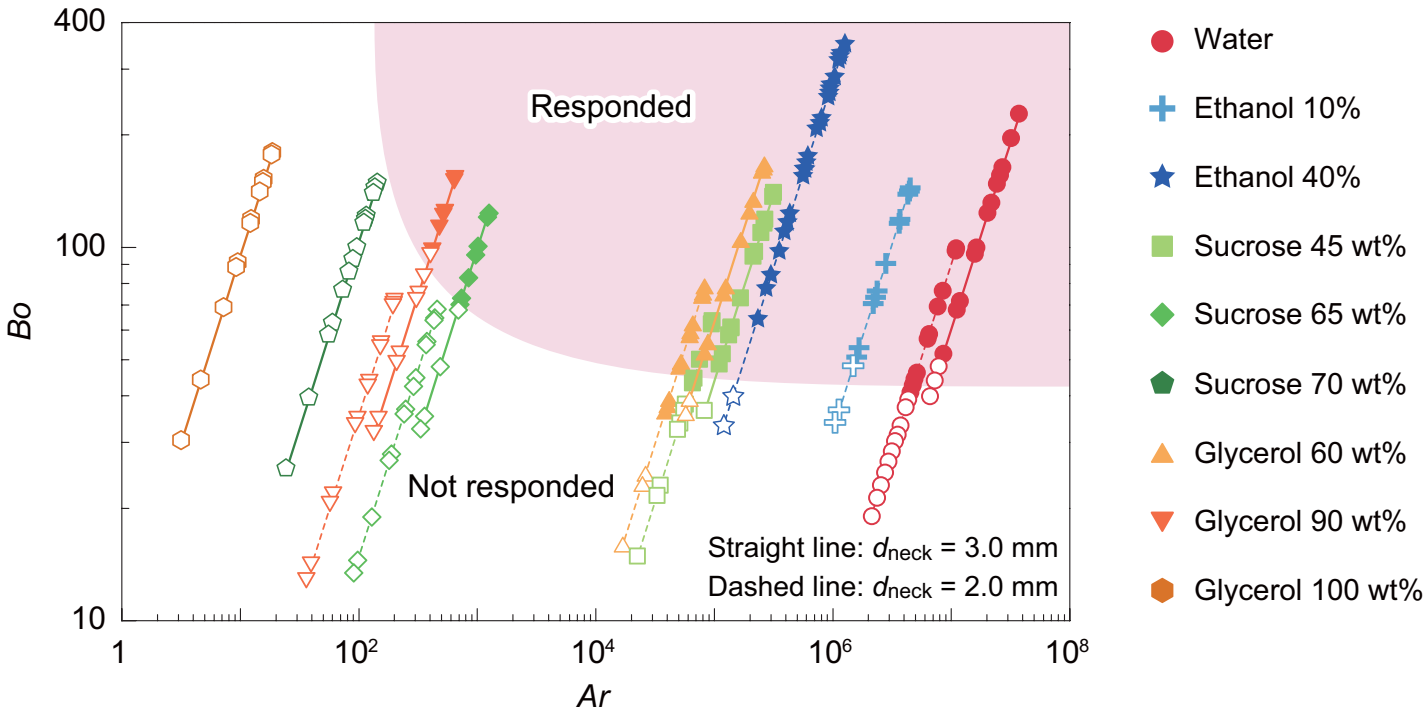

Fig 8. State diagram of the response of the sensor as a function of *Ar* and *Bo*. Filled symbols represent sensors that "responded," while open symbols represent sensors that "did not respond." Circle: water, cross: ethanol 10%, star: ethanol 40%, square: sucrose 45 wt%, diamond: sucrose 65 wt%, pentagon: sucrose 70 wt%, triangle: glycerol 60 wt%, inverse triangle: glycerol 90 wt%, and hexagon: glycerol. Straight and dashed lines represent the results obtained with d_{neck} = 3.0 mm and 2.0 mm, respectively.

https://doi.org/10.1371/journal.pone.0195741.g008

respond because the aqueous droplet could no longer be elongated instantaneously owing to the strong damping effect. The regime where the sensors respond is highlighted in the figure.

Conclusion

We showed that our simple impact sensor that was implemented without the use of electronics but with the use of plastic housing and working fluids only, can detect impacts (instantaneous accelerations) above certain thresholds. We fabricated and tested the prototype sensor, and established the basic design and choice of the working fluids so that the sensor covers the 30 to 100 g range that is relevant and applicable to human body or head impacts in various sports. We systematically tested the effect of the neck size and fluid parameters (density, viscosity, and interfacial tension), and discussed how these parameters influenced the threshold value. Analysis of the elicited results based on nondimensional numbers provided a useful guideline for the design of the sensor for various applications. Among these parameters, the viscosity of the aqueous droplet was the easiest controllable parameter since it could be readily tuned by additives. The viscosity of the oil could be a possible choice, but it depended on the availability of the types of oil with various viscosities. Hydrocarbon oil and silicone oils have various chain lengths and viscosities, but their densities were close to water (~0.7 g/ml and ~1.0 mg/ml, respectively). This property makes them less attractive because it reduces the relative inertial force on water. The size of the neck was also an easily changeable parameter, but it directly changed the size of the droplet after it pinched off. If its size was too small, the visual judgment was more difficult. The interfacial tension value could be the best choice since it can be tuned using surfactants. However, we did not test these variables in the present work because of the

difficulty encountered in obtaining good surfactants for fluorocarbon oil. The long-term stability of the water/oil interfacial tension value could also be a problem in terms of its practical use.

Although we established that the basic design and physical mechanism of operation of our proposed sensor, there are still many issues that have to be considered. One of them is the directionality of sensing. A water droplet immersed in fluorocarbon oil tends to float so that it is always in contact with the neck cavity. However, when one aims to detect the acceleration in a direction that is not parallel to gravity, then one cavity has to be completely packed with water droplets so that the interface is always in contact with the entrance of the neck. Although we only tested the single-axis sensor, multidirectional detection could be implemented by the appropriate design of the housing. Connecting the donut-shape cavity to the center cavity with a droplet will allow this device to be able to detect 2D impacts. Another important issue is the shelf life. The packaging and hermeticity of our handmade prototype was imperfect, and an air bubble gradually grew in the cavity within several days that deteriorated the reproducibility of the detection. Mass production with the plastic molding and automated fluid injection system should solve this problem. We are currently working on these issues to develop a more practical version of this impact sensor.

Although it is still in a primitive stage, we believe that the development of this extremely low-cost impact sensor without the use of electronics would benefit certain real-life applications, such as sports and logistics. It is envisaged to be particularly useful and important in sports where quantitative data can be obtained to evaluate safety. The appropriate safety measure should be enforced for professional and high-level players and for amateurs, including players at younger ages. Our efforts to identify suitable usages and appropriate configurations in practical applications are ongoing.

Supporting information

S1 Fig. Characterization of the custom-made falling apparatus. (a) Dependence of the peak acceleration values on the drop height. (b) Dependence of the duration of acceleration profile on the drop height.
(EPS)

S2 Fig. Scatter plot of the diameter of separated droplets. Diameters measured in each falling experiments with different neck diameters are plotted versus each acceleration value.
(EPS)

S3 Fig. State diagram of the response of the sensor as a function of Reynolds number and Weber number. This plot shows inconsistent responses among different experimental conditions but within similar regions.
(EPS)

S1 Table. Parameters of curve fitting results for all experimental data presented in Figs 4–7.
(XLSX)

Acknowledgments

This research was supported by JKA and its promotion funds from KEIRIN RACE (27–120). We also thank Prof. T. Komine and Prof. I. Dan in Chuo University, and Mr. T. Hoshino for valuable discussions.

Author Contributions

Conceptualization: Hiroaki Suzuki.

Data curation: Daigo Takahashi, Taiji Okano, Hiroaki Suzuki.

Funding acquisition: Taiji Okano.

Investigation: Daigo Takahashi, Keisuke Hara, Taiji Okano.

Project administration: Hiroaki Suzuki.

Writing – original draft: Daigo Takahashi, Taiji Okano, Hiroaki Suzuki.

Writing – review & editing: Hiroaki Suzuki.

References

1. Barbour N, Schmidt G. Inertial sensor technology trends. IEEE Sens J. 2001; 1(4):332–339. https://doi.org/10.1109/7361.983473
2. Yang CC, Hsu YL. A review of accelerometry-based wearable motion detectors for physical activity monitoring. Sensors. 2010; 10(8):7772–7788. https://doi.org/10.3390/s100807772 PMID: 22163626
3. Allet L, Knols RH, Shirato K, de Bruin ED. Wearable systems for monitoring mobility-related activities in chronic disease: a systematic review. Sensors. 2010; 10(10):9026–9052. https://doi.org/10.3390/s101009026 PMID: 22163393
4. Zeng HS, Zhao Y. Sensing movement: microsensors for body motion measurement. Sensors. 2011; 11 (1):638–660. https://doi.org/10.3390/s110100638 PMID: 22346595
5. del Rosario MB, Redmond SJ, Lovell NH. Tracking the evolution of smartphone sensing for monitoring human movement. Sensors. 2015; 15(8):18901–18933. https://doi.org/10.3390/s150818901 PMID: 26263998
6. Hernandez W. A survey on optimal signal processing techniques applied to improve the performance of mechanical sensors in automotive applications. Sensors. 2007; 7(1):84–102. https://doi.org/10.3390/S7010084
7. Wang Y, Fan JB, Zu J, Xu P. Quasi-static calibration method of a high-g accelerometer. Sensors. 2017; 17(2). https://doi.org/10.3390/S17020409 PMID: 28230743
8. Vannoni M, Straulino S. Low-cost accelerometers for physics experiments. Eur J Phys. 2007; 28(5):781–787. https://doi.org/10.1088/0143-0807/28/5/001
9. Duma SM, Rowson S. Past, present, and future of head injury research. Exercise and sport sciences reviews. 2011; 39(1):2–3. https://doi.org/10.1097/JES.0b013e318203dfdb PMID: 21183827.
10. McIntosh AS, Patton DA, Frechede B, Pierre PA, Ferry E, Barthels T. The biomechanics of concussion in unhelmeted football players in Australia: a case-control study. BMJ Open. 2014; 4(5). https://doi.org/10.1136/bmjopen-2014-005078 PMID: 24844272
11. King D, Hume PA, Brughelli M, Gissane C. Instrumented mouthguard acceleration analyses for head impacts in amateur rugby union players over a season of matches. The American journal of sports medicine. 2015; 43(3):614–624. https://doi.org/10.1177/0363546514560876 PMID: 25535096.
12. Wilcox BJ, Beckwith JG, Greenwald RM, Chu JJ, McAllister TW, Flashman LA, et al. Head impact exposure in male and female collegiate ice hockey players. J Biomechanics. 2014; 47(1):109–114. https://doi.org/10.1016/j.jbiomech.2013.10.004 PMID: 24210478.
13. Gwin JT, Chu JJ, McAllister TA, Greenwald RM. In situ measures of head impact acceleration in NCAA division I men's ice hockey: Implications for ASTM F1045 and other ice hockey helmet standards. Am Soc Test Mater. 2009; 1516:244. https://doi.org/10.1520/Jai101848
14. Green GA, Jordan SE. Are brain injuries a significant problem in soccer? Clin Sport Med. 1998; 17 (4):795–809. https://doi.org/10.1016/S0278-5919(05)70120–70124
15. Pickett W, Streight S, Simpson K, Brison RJ, Cusimano M. Head injuries in youth soccer players presenting to the emergency department. Brit J Sport Med. 2005; 39(4):226–231. https://doi.org/10.1136/bjsm.2004.013169 PMID: 15793093
16. Murayama H, Hitosugi M, Motozawa Y, Ogino M, Koyama K. Simple strategy to prevent severe head trauma in Judo –Biomechanical analysis–. Neurol Med-Chir. 2013; 53(9):580–584.

17. Camarillo DB, Shull PB, Mattson J, Shultz R, Garza D. An instrumented mouthguard for measuring linear and angular head impact kinematics in American football. Annals of biomedical engineering. 2013; 41(9):1939–1949. https://doi.org/10.1007/s10439-013-0801-y PMID: 23604848.

18. Swartz EE, Broglio SP, Cook SB, Cantu RC, Ferrara MS, Guskiewicz KM, et al. Early results of a helmetless-tackling intervention to decrease head impacts in football players. J Athletic Training. 2015; 50 (12):1219–22. https://doi.org/10.4085/1062-6050-51.1.06 PMID: 26651278.

19. King DA, Hume PA, Gissane C, Clark TN. Similar head impact acceleration measured using instrumented ear patches in a junior rugby union team during matches in comparison with other sports. J Neurosurg-Pediatr. 2016; 18(1):65–72. https://doi.org/10.3171/2015.12.PEDS15605 PMID: 26942267

20. Duma SM, Manoogian SJ, Bussone WR, Brolinson PG, Goforth MW, Donnenwerth JJ, et al. Analysis of real-time head accelerations in collegiate football players. Clinical J Sport Medicine. 2005; 15(1):3–8. PMID: 15654184.

21. Greenwald RM, Gwin JT, Chu JJ, Crisco JJ. Head impact severity measures for evaluating mild traumatic brain injury risk exposure. Neurosurgery. 2008; 62(4):789–798. https://doi.org/10.1227/01.neu.0000318162.67472.ad PMID: 18496184.

22. Gardner AJ, Kohler RM, Levi CR, Iverson GL. Usefulness of video review of possible concussions in national youth Rugby league. Int J Sports Medicine. 2017; 38(1):71–75. https://doi.org/10.1055/s-0042-116072 PMID: 27737484.

23. Krolikowski MP, Black AM, Palacios-Derflingher L, Blake TA, Schneider KJ, Emery CA. The effect of the "zero tolerance for head contact" rule change on the risk of concussions in youth ice hockey players. American J Sports Medicine. 2017; 45(2):468–473. https://doi.org/10.1177/0363546516669701 PMID: 27789471.

24. Smith AM, Gaz DV, Larson D, Jorgensen JK, Eickhoff C, Krause DA, et al. Does fair play reduce concussions? A prospective, comparative analysis of competitive youth hockey tournaments. BMJ open sport & exercise medicine. 2016; 2(1):e000074. https://doi.org/10.1136/bmjsem-2015-000074 PMID: 27900157.

25. Hasegawa K, Takeda T, Nakajima K, Ozawa T, Ishigami K, Narimatsu K, et al. Does clenching reduce indirect head acceleration during rugby contact? Dent Traumatol. 2014; 30(4):259–264. https://doi.org/10.1111/edt.12082 PMID: 24138128

26. Buzas D, Jacobson NA, Morawa LG. Concussions From 9 Youth Organized Sports: Results from NEISS hospitals over an 11-year time frame, 2002–2012. Orthopaedic J Sports Medicine. 2014; 2 (4):2325967114528460. https://doi.org/10.1177/2325967114528460 PMID: 26535315.

27. Linzmeier KA, LaBella CR. Concussions in collision youth sports. Pediatric Neurology Briefs. 2016; 30 (1):3. https://doi.org/10.15844/pedneurbriefs-30-1-2 PMID: 27004137.

28. Rivara FP, Graham R. Sports-related concussions in youth: report from the Institute of Medicine and National Research Council. Jama. 2014; 311(3):239–240. https://doi.org/10.1001/jama.2013.282985 PMID: 24185195.

29. Marar M, McIlvain NM, Fields SK, Comstock RD. Epidemiology of concussions among United States high school athletes in 20 sports. American J Sports Medicine. 2012; 40(4):747–755. https://doi.org/10.1177/0363546511435626 PMID: 22287642.

30. Broglio SP, Sosnoff JJ, Shin S, He X, Alcaraz C, Zimmerman J. Head impacts during high school football: a biomechanical assessment. J Athletic Training. 2009; 44(4):342–349. https://doi.org/10.4085/1062-6050-44.4.342 PMID: 19593415.

31. Funk JR, Rowson S, Daniel RW, Duma SM. Validation of concussion risk curves for collegiate football players derived from HITS data. Annals Biomed Eng. 2012; 40(1):79–89. https://doi.org/10.1007/s10439-011-0400-8 PMID: 21994060.

32. Liu SQ, Zhu R. Micromachined Fluid Inertial Sensors. Sensors. 2017; 17(2). https://doi.org/10.3390/S17020367 PMID: 28216569

33. Varga M, Ladd C, Ma S, Holbery J, Troster G. On-skin liquid metal inertial sensor. Lab Chip. 2017. https://doi.org/10.1039/c7lc00735c PMID: 28836638.

34. Zeng H, Zhao Y. Dynamic behavior of a liquid marble based accelerometer. Appl Phys Lett. 2010; 96 (11). https://doi.org/10.1063/1.3367704

35. Zeng HS, Zhao Y. Liquid-state motion sensing. Sensor Actuat B. 2011; 154(1):33–40. https://doi.org/10.1016/j.snb.2009.11.069

36. Broglio SP, Eckner JT, Kutcher JS. Field-based measures of head impacts in high school football athletes. Current Opinion in Pediatrics. 2012; 24(6):702–708. https://doi.org/10.1097/MOP.0b013e3283595616 PMID: 23042253.

37. Guskiewicz KM, Mihalik JP. Biomechanics of sport concussion: quest for the elusive injury threshold. Exercise and Sport Sciences Reviews. 2011; 39(1):4–11. https://doi.org/10.1097/JES.0b013e318201f53e PMID: 21088602.

38. Cobb BR, Urban JE, Davenport EM, Rowson S, Duma SM, Maldjian JA, et al. Head impact exposure in youth football: elementary school ages 9–12 years and the effect of practice structure. Annals Biomed Eng. 2013; 41(12):2463–2473. https://doi.org/10.1007/s10439-013-0867-6 PMID: 23881111.

39. Riches PE. A dynamic model of the head acceleration associated with heading a soccer ball. Sports Engineering. 2006; 9:39–47.

40. Deng X, Schellenberger F, Papadopoulos P, Vollmer D, Butt HJ. Liquid drops impacting superamphiphobic coatings. Langmuir. 2013; 29(25):7847–7856. https://doi.org/10.1021/la401120j PMID: 23697383

41. Mazutis L, Griffiths AD. Selective droplet coalescence using microfluidic systems. Lab Chip. 2012; 12 (10):1800–1806. https://doi.org/10.1039/c2lc40121e PMID: 22453914

42. Utada AS, Fernandez-Nieves A, Stone HA, Weitz DA. Dripping to jetting transitions in coflowing liquid streams. Phys Rev Lett. 2007; 99(9). https://doi.org/10.1103/Physrevlett.99.094502 PMID: 17931011